

Quantum Confocal Microscopy in Fock Space with a 19 dB Metrological Gain

Ziyue Hua,^{1,*} Chuanlong Ma,^{1,*} Yilong Zhou,^{1,*} Yifang Xu,¹ Zi-Jie Chen,² Weizhou Cai,² Jiajun Chen,¹ Lintao Xiao,¹ Hongwei Huang,¹ Weiting Wang,¹ Hekang Li,^{3,4} Haohua Wang,^{3,4} Ming Li,^{2,4,†} Chang-Ling Zou,^{2,4,‡} and Luyan Sun^{1,4,§}

¹Center for Quantum Information, Institute for Interdisciplinary Information Sciences, Tsinghua University, Beijing 100084, China

²Laboratory of Quantum Information, University of Science and Technology of China, Hefei 230026, China

³School of Physics and ZJU-Hangzhou Global Scientific and Technological Innovation Center, Zhejiang University, Hangzhou 310027, China

⁴Hefei National Laboratory, Hefei 230088, China

Quantum metrology promises measurement precision beyond classical limits by exploiting large-scale quantum states, yet realizing this advantage faces two fundamental challenges: the deterministic preparation of non-trivial quantum probes and the efficient extraction of metrological information in high-dimensional Hilbert spaces. Here, we introduce quantum confocal microscopy in Fock space that simultaneously resolves both challenges. Drawing a direct analogy between classical wave optics and quantum state evolution in a bosonic mode, we construct a confocal system with two Fock-space lenses. The first lens deterministically focuses a coherent state into a quantum probe with a tightly concentrated photon-number distribution, while the second lens maps the metrological information back to the vacuum state for efficient readout. Using a superconducting circuit QED platform, we prepare focused probe states with mean photon numbers up to $N = 500$, achieving a 21.5 ± 1.1 dB compression of the photon-number uncertainty relative to a coherent state, with a scalable quantum circuit of $\mathcal{O}(1)$ operational depth. We demonstrate a displacement sensitivity scaling as $N^{-0.416}$, approaching the Heisenberg scaling ($N^{-0.5}$), and achieve a record metrological gain of 19.06 ± 0.13 dB beyond the standard quantum limit. This work establishes quantum confocal microscopy as a scalable and practical framework for quantum-enhanced precision measurement, readily extendable to other bosonic platforms and high-dimensional quantum many-body systems.

I. INTRODUCTION

The enhancement of measurement precision holds profound significance across diverse scientific and technological domains, ranging from the discovery of new physics to the foundation of international standards [1–3]. Quantum metrology, which leverages the superposition and entanglement of large numbers of microscopic particles or excitations, is expected to significantly improve measurement precision beyond the standard quantum limits (SQLs) [4–9]. Two complementary platforms have been exploited to validate the principles of quantum metrology. In ensembles of two-level systems, collectively entangled quantum states, such as spin-squeezed states [10, 11], GHZ states [12, 13], and spin-motion entanglement states [14, 15], have demonstrated quantum-enhanced measurement precision. Bosonic modes offer a distinct advantage of demonstrating large-scale quantum properties with reduced hardware complexity by exploiting the infinite-dimensional Hilbert space of harmonic oscillators [16, 17]. The metrological capability of bosonic modes has been investigated utilizing Fock states and their superpositions [18–22], cat states [23–25], and NOON states [26, 27], positioning the bosonic modes as a promising platform for practical quantum-enhanced sensing.

Despite these advances, two fundamental challenges obstruct the practical realization of large metrological gains in macroscopic quantum systems. The first is state preparation. While metrological precision improves with the number of particles or excitations N , the preparation of high non-trivial quantum probe states becomes exponentially more demanding as N grows [28, 29]. In bosonic modes, for instance,

photon injection [30–33] and pulse engineering [34–38], require increasingly complex quantum circuits whose depth and gate count scale with N , making them highly susceptible to decoherence and practical imperfections. Non-deterministic approaches relying on ancilla qubit measurements can reach 100 photons [22, 39], but their success probability dramatically drops with increasing N . The second bottleneck is information extraction. Even when such large-scale quantum states can be prepared, the efficient extraction of metrological information from these complex, high-dimensional probe states after interrogation remains challenging. One possible approach is to construct a time-reversal evolution of the system, either through Hamiltonian inversion [40–42] or echo-type processes [11, 15, 43], which maps the probe state back near a simple reference state for efficient readout. However, such approaches demand precise control over the Hamiltonian of the entire quantum system, placing stringent and often impractical requirements on experiment.

Here, we propose and experimentally demonstrate “quantum confocal microscopy”, a paradigm that simultaneously resolves the challenges in efficient generation and detection of certain non-classical states in high-dimensional Hilbert spaces. Drawing a direct analogy between classical wave optics and quantum state evolution in a bosonic mode, we construct a 4f confocal system using lenses in Fock space. This architecture deterministically focuses a readily generated large coherent state into a non-classical Fock-space-focused (N -focused) state characterized by sharply compressed photon-number uncertainty [44, 45]. The confocal microscopy is inherently scalable with a constant operational depth $\mathcal{O}(1)$. We experimentally prepare N -focused states with a mean photon number up to 500 and a central Fock-state pop-

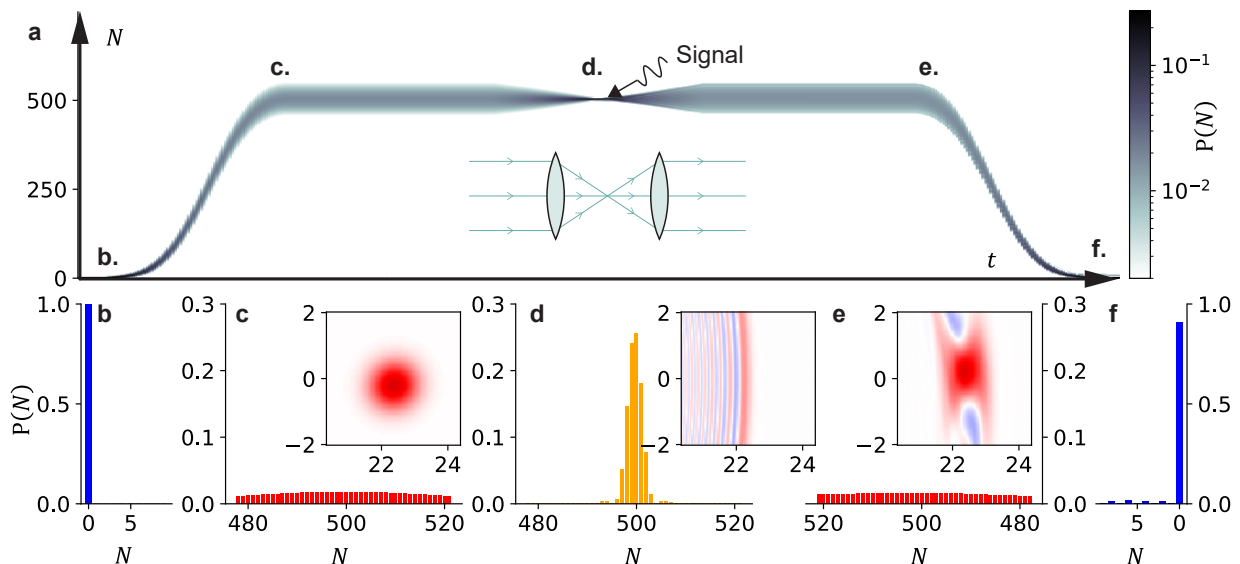


FIG. 1: **Fock-space confocal system for state preparation and detection.** **a**, Changes of photon-number distribution during the Fock-space confocal circuit. The circuit maps a coherent state back to an approximate coherent state using two Fock-space convex lenses with the same focal point, analogous to the confocal convex lens system in optics. **b-f**, Close-up of photon-number distribution at various moments. **b**, At the starting point, the system is in the vacuum state, with all population being in the Fock state $|0\rangle$. **c**, A displacement transformation maps the vacuum state to a coherent state with 500 average photons and a broad distribution. The inset shows the Wigner distribution of the coherent state. **d**, After passing through a Fock-space convex lens, the coherent state is focused into an N -focused state, with photon-number distribution tightly concentrated around several Fock states near $N = 500$. The inset shows the Wigner distribution of the N -focused state, which has fine fringes for detecting small signals. **e**, After passing through another Fock-space convex lens, the N -focused state diverges into a coherent-like state, with a broad photon-number distribution. The inset shows its Wigner distribution, which is generally similar to that of a coherent state except for slight distortions. **f**, A final backward displacement transformation maps the coherent-like state to a near vacuum state. Theoretically, over 90% of the population returns to the vacuum state, facilitating efficient state measurement.

ulation surpassing 20%. Crucially, by leveraging the confocal architecture, we achieve approximate time-reversal via a secondary Fock-space convex lens, remapping the N -focused state near a coherent state for simple and efficient information extraction. This deterministic confocal metrology circuit achieves an information extraction efficiency exceeding 90%, showing a quantum-enhanced metrological gain of 19.06 dB beyond SQL. Our work establishes a scalable framework for preparing large-scale non-classical states, marking a critical step toward quantum-enhanced sensing technologies.

II. RESULTS

A. Confocal system in Fock space

Figure 1(a) illustrates the concept of quantum confocal microscopy in Hilbert space. It shows the evolution of a bosonic mode quantum state throughout the quantum circuit, with the state distribution along the photon-number basis. The inset depicts the corresponding classical $4f$ confocal system widely used in optical microscopy, which consists of two lenses with coincident focal points. The first lens transforms a broad collimated beam into a tight, diffraction-limited focal spot, while the second lens re-collimates the beam, enabling high resolution and efficient signal collection. Building on an equiv-

alence between optical wave propagation in real space and quantum state evolution in Fock space (Supplementary Section I A) [44, 45], coherent states as a Gaussian beam in Fock space can be focused into N -focused states and subsequently remapped back to a coherent state near the vacuum (Supplementary Section I B).

The principle of the quantum confocal microscopy is numerically simulated and illustrated in Figs. 1(b-e), with a constant operation depth independent of N . Initially, the bosonic mode resides in the vacuum state, with its photon-number distribution shown in Fig. 1(b). A large displacement operation first converts the vacuum state into a coherent state with an average photon number $\bar{N} = 500$, with photon-number distributions and Wigner functions depicted in Fig. 1(c). Subsequently, a Fock-space convex lens, composed of sequential quadratic phase accumulation followed by weak-driving evolution, transforms the coherent state into an N -focused state, as shown in Fig. 1(d). A second lens with identical parameters and a common focal point then reconverts the N -focused state into a quasi-coherent state, as shown in Fig. 1(e). These numerical results validate bidirectional state conversion between coherent and N -focused states via the confocal architecture, confirming our optical intuition. The photon-number distribution of the quasi-coherent state closely resembles the coherent state, while minor distortions in the Wigner function arise from the inherent discrete nature of Fock-space (see

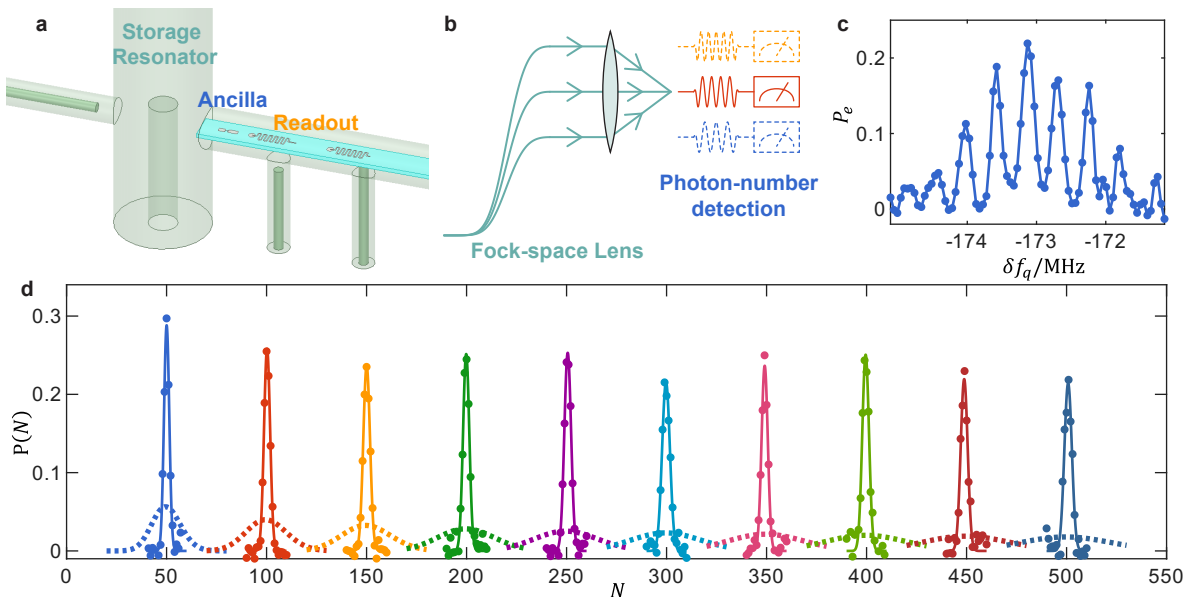


FIG. 2: **Scaling of N -focused state.** **a**, Schematic of the superconducting circuit QED setup: a 3D cavity coupled to a transmon qubit and a readout resonator. **b**, The circuit of preparing and calibrating the N -focused states. The N -focused state is prepared by compressing a coherent state through a convex Fock-space lens, then calibrated with a photon number selection pulse and measurement of the transmon qubit. **c**, Ancilla-qubit-assisted detection results for an N -focused state with an average photon number of $\bar{N} = 300$. **d**, Measured $P(N)$ (dots) and Gaussian fits (solid lines) for the N -focused state at various \bar{N} from 50 to 500, demonstrating deep sub-Poissonian statistics compared to coherent states (dashed lines). The peak probability and the width of the distribution remain nearly the same at various target photon numbers, confirming the scalability of the state preparation process.

Supplementary Section I C). Finally, a reverse large displacement operation repositions the quasi-coherent state near the vacuum origin, with the resulting photon-number distribution shown in Fig. 1(f).

The N -focused state exhibits the fundamental quantum enhancement for metrological gain beyond SQL. As shown in Fig. 1(d), experimental feasible parameters allow compression of the photon-number distribution to a narrow full width at half maximum (FWHM) of around 4 photons for $\bar{N} = 500$. In particular, the population on the Fock state $|N = 500\rangle$ with a deterministic photon number exceeds 20%. The Wigner distribution of the N -focused state (inset of Fig. 1(d)) reveals dense, ring-like fringes analogous to those of Fock states, confirming the high-precision metrological capability [16], in contrast to the coherent state in Fig. 1(c). Moreover, the negativity of the Wigner distribution demonstrates that the N -focused state is non-Gaussian, distinguishing it from conventional squeezed states.

Another key advantage of this confocal design is that it resolves the information readout bottleneck. Rather than directly measuring the macroscopic post-sensing state, this approach employs a second Fock-space lens followed by a reverse displacement to implement an approximate time-reversal. This maps the complex state imprinted with the test perturbation back near the vacuum state $|0\rangle$, converting the tiny shift at the “focus” into a simple observable change near vacuum. Simulations show that over 90% of the population returns to the vacuum state in the absence of test perturba-

tion, correlating the magnitude of mid-circuit perturbations with the change in the final vacuum-state fidelity and enabling precise signal detection. Thus, information is extracted via efficient near-vacuum measurements, circumventing the need for macroscopic quantum state tomography. Crucially, unlike conventional time-reversal protocols that require precise Hamiltonian inversion ($H \rightarrow -H$) [40–42], our protocol, analogous to classical optics, requires no such inversion and is inherently robust.

B. Characterization of the Fock lens and confocal system

Our circuit quantum electrodynamics (QED) system [46–48] consists of three key components: a high-quality memory resonator stores quantum information, an ancilla transmon qubit, and a readout resonator, as shown in Fig. 2(a). The storage resonator features a long lifetime of 2.8 ms and acquires Kerr nonlinearity via coupling with the ancilla qubit. The dispersive coupling between the ancilla qubit and the storage resonator causes frequency shifts on the qubit when the storage resonator is in specific Fock states. Therefore, applying frequency-selective drives on the qubit can distinguish different Fock states in the resonator [49]. The readout resonator, with a short lifetime ($< 1 \mu\text{s}$), is also dispersively coupled to the ancilla qubit. We measure the state of the ancilla qubit by performing homodyne detection on the readout resonator. Detailed system parameters and wiring are given in Supple-

mentary Section II.

The photon-number distribution of the N -focused state is calibrated by qubit-assisted photon-number detection. We first prepare an N -focused state in the storage cavity using the circuit illustrated in Figs. 1(b-d). Then, frequency-selective π -pulses are applied to the ancilla qubit at varying frequencies, and successful qubit flips are identified by reading out the ancilla qubit through the readout resonator, as shown in Fig. 2(b). Figure 2(c) presents the detection results for an N -focused state with an average photon number of $\bar{N} = 300$. The qubit excitation is detectable only when the cavity has population in a specific Fock state, and the qubit drive frequency aligns with the transition frequency corresponding to that Fock state. By systematically preparing N -focused states with different average photon numbers and analyzing the qubit excitation peak positions one by one, we identify the transition frequencies of specific Fock states within the cavity (Supplementary Section II D). Furthermore, applying a set of distinct qubit drive frequencies to a given N -focused state allows quantification of the population distribution across its Fock state components.

We demonstrate the scalability of the Fock-space focusing circuit by measuring the photon-number distributions of the N -focused states at various average photon numbers \bar{N} , as shown in Fig. 2(d). The solid lines represent Gaussian fits to the experimental data, while the dashed lines correspond to coherent states with matching \bar{N} . As \bar{N} increases, the prepared N -focused state distributions remain essentially stable, whereas the coherent state distributions broaden proportionally to $\sqrt{\bar{N}}$. We fit the distribution of the N -focused state with Gaussian function $P(N) = A \cdot \exp(-(N - \bar{N})^2/(2\sigma^2))$, as shown by the dashed lines in Fig. 2(d). The fitted standard deviation σ is smaller than 2 photons for all \bar{N} , consistent with the theoretical prediction (Supplementary Section IV A). At $\bar{N} = 500$, the central occupation of the N -focused state remains above 20%, with a fitted $\sigma = 1.9 \pm 0.3$ photons, corresponding to a 21.5 ± 1.1 dB compression compared to coherent states. However, the measurement fidelity of the ancilla qubit degrades with increasing photon numbers, resulting in elevated noise levels in the experimental data (Supplementary Section II D). The limited fidelity of direct measurement not only restricts potential post-measurement selection operations, but also limits the precision of directly applying N -focused states for quantum metrology.

As a reversal of the preparation of N -focused state, the Fock-space lens can be applied to detect the projection of state on a N -focused state. Figure 3(a) shows detection channels with varying mean photon numbers, which could serve as basis vectors for quantum state tomography, enabling precise photon-number distribution measurement of an input state, termed Fock-space scanning tomography (N -tomo). In this scheme, an arbitrary initial state undergoes a convex lens and displacement operation. The N -focused state component within the initial state is mapped near the vacuum state, allowing quantification of the N -focused component fraction in the initial state by measuring the vacuum-state proportion (Sup-

plementary Section III A).

We experimentally demonstrate the reconstruction of photon-number distributions from N -tomo results for various initial states, along with their corresponding theoretical distributions and Wigner distributions, as shown in Figs. 3(b-i). We first reconstruct the photon-number distribution of the N -focused state using its N -tomo results, as shown in Figs. 3(b-c). Based on the reconstructed distribution of the N -focused state, we subsequently reconstruct the photon-number distributions of other unknown pure states from their N -tomo results, with detailed methods provided in the Supplementary Section III D.

Specifically, we apply N -tomo to the coherent state $\mathcal{D}[\sqrt{n_t}]|0\rangle$, parallel-displaced cat (PDC) state $\mathcal{D}[\sqrt{n_t}](|\alpha\rangle + |-\alpha\rangle)/\sqrt{2}$ and orthogonal-displaced cat (ODC) state $\mathcal{D}[\sqrt{n_t}](|i\alpha\rangle + |-i\alpha\rangle)/\sqrt{2}$. The state preparation protocol is detailed in Supplementary Section III B. We choose $n_t = 100$ and $\alpha = 2$ as an example. The coherent state has a wide Gaussian-like photon-number distribution centered at $n_t = 100$, as shown in Figs. 3(d-e). The PDC state has two coherent state components with significantly different average photon numbers (64 and 144 photons), as shown in Figs. 3(f-g). The ODC state consists of two coherent states with identical average photon numbers (104 photons) but a relative phase difference, resulting in a characteristic triple-peak structure in the photon-number distribution, as shown in Figs. 3(h-i). Experimentally reconstructed results for all types of states agree well with theoretical predictions, confirming that N -tomo not only possesses a broad detection range but also exhibits high resolution for fine structures in photon-number distributions arising from coherent superpositions.

C. Quantum sensing of displacement

We now integrate the preparation and detection protocols of N -focused states to achieve quantum-enhanced metrology. The protocol employs a confocal system where a small, unknown displacement $D(\beta)$ is applied at the focal point. The displacement magnitude information is extracted by measuring the final vacuum-state probability $P(0)$. To calibrate the detector response, we first apply a known displacement β_0 and scan its intensity. Figure 4(a) demonstrates the experimental measurement results of $P(0)$, with distinct color points representing results for different average photon numbers ($\bar{N} = 50, 200, 350, 500$). Black points represent coherent-state probe measurement results, corresponding to the SQL in our system. Notably, the confocal system demonstrates a significantly steeper slope than that of a coherent state.

To extract the information in the measurement result, we first fit the experimental data with a Gaussian function $P(0|\beta) = A \cdot \exp(-\beta^2/(2\sigma^2)) + C$ (dashed lines in Fig. 4(a)). The fitting curves agree well with the experimental data. We then calculate the classical Fisher information (CFI) using the formula $I_c(\beta) = (\partial P(0|\beta)/\partial \beta)^2 / (P(0|\beta)(1 -$

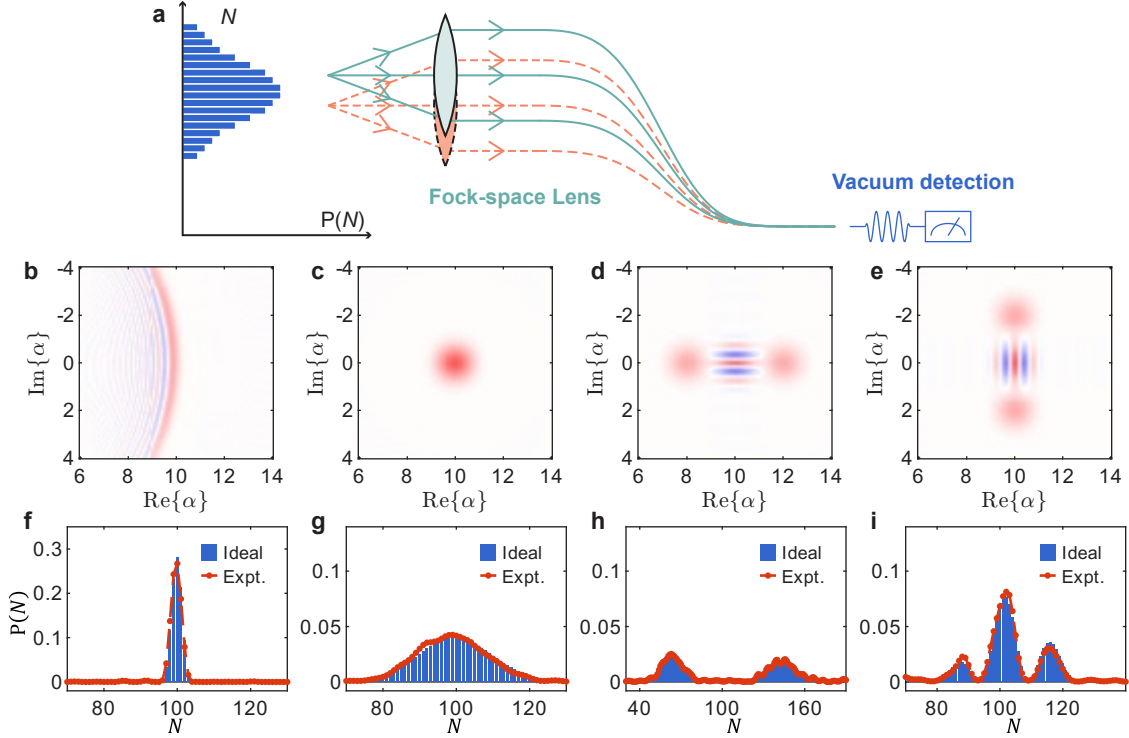


FIG. 3: **Fock-space scanning tomography (N -tomo) of various states.** **a**, The circuit of calibrating an unknown target state with N -tomo. The target state passes through a Fock-space convex lens and then a displacement operation, followed by measuring the vacuum probability of the final state. The N -tomo circuit maps the N -focused state component in the target state back to the vacuum state, similar to the optical conjugation of the N -focused state preparation circuit. By adjusting the circuit parameters, the N -tomo circuit can detect the proportions of different N -focused components in the target state, thereby reconstructing the photon-number distribution. **b-e**, The theoretical Wigner distribution of the N -focused state, the coherent state, the parallel-displaced cat (PDC) state, and the orthogonal-displaced cat (ODC) state. **f-i**, The ideal and reconstructed photon-number distribution of each state. The distribution of the N -focused state is used for reconstructing other unknown states. The PDC state has two components with different photon numbers, resulting in a two-peak photon-number distribution. The ODC state has two components with the same photon numbers, resulting in a three-peak photon-number distribution. The N -tomo results clearly capture the difference between PDC and ODC states.

$P(0|\beta)$), and the results are shown in Fig. 4(b). The results show that $I_c(\beta)$ for our confocal metrology circuit peaks at specific optimal bias points β_0 for various average photon numbers \bar{N} . At $\bar{N} = 350$, the maximum CFI reaches $3.22 \pm 0.10 \times 10^2$ at $\beta_0 = 0.055$, surpassing the ideal SQL ($I_c = 4$) by a factor of 80.5.

To intuitively visualize the origin of sensing enhancement, we characterize the population distribution of the lowest few Fock components in the final output states, as shown in Fig. 4(c). We select the operating point with the highest precision at $\bar{N} = 350$ and bias the system at $\beta_0 = 0.055$, where the CFI is maximized. The populations of Fock components with photon numbers $N \leq 10$ are presented as solid bars in Fig. 4(c). When a test drive differs from the bias point by $\Delta\beta = \pm 0.02$, the changed Fock populations are shown as hollow bars in Fig. 4(c). The vacuum-state ($|0\rangle$) population exhibits a significant variation when the test drive is applied. For comparison, Fig. 4(d) shows the final state population changes of a coherent-state probe at its optimal bias $\beta_0 = 0.515$. Under the same test drive strength, the variation of the final state in the confocal metrology circuit is remarkably larger than

that of the coherent-state circuit. Due to system imperfections such as aberrations and dissipation, not all population returns to the vacuum state after one confocal circuit, resulting in a gradually decreasing distribution across the Fock states $|1\rangle$ to $|10\rangle$ and a residual population in states $|N > 10\rangle$. We observe that the populations in Fock states $|1 \leq N \leq 10\rangle$ also vary with the test drive strength, suggesting that quantum information might be partially recovered via error correction or mitigation techniques. For instance, one can construct low-Fock-number operations with numerically optimized pulse shaping to transfer more population on the Fock states $|1 \leq N \leq 10\rangle$ back to $|0\rangle$, thereby enhancing the metrology performance.

According to the Cramér-Rao theorem, the minimum achievable uncertainty $\delta\beta$ for the test small displacement β can be directly obtained from the CFI of the measurement result, i.e., $\delta\beta = 1/\sqrt{I_c}$. Figure 4(e) plots the measured displacement uncertainty, $\delta\beta$, as a function of the mean photon number \bar{N} on a log-log scale. The sensitivity improves rapidly as \bar{N} increases. For comparison, an ideal coherent state can only yield $|\delta\beta| \geq 0.5$ regardless of the number of photons used, representing the SQL as $\delta\beta_{\text{SQL}} = 0.5$,

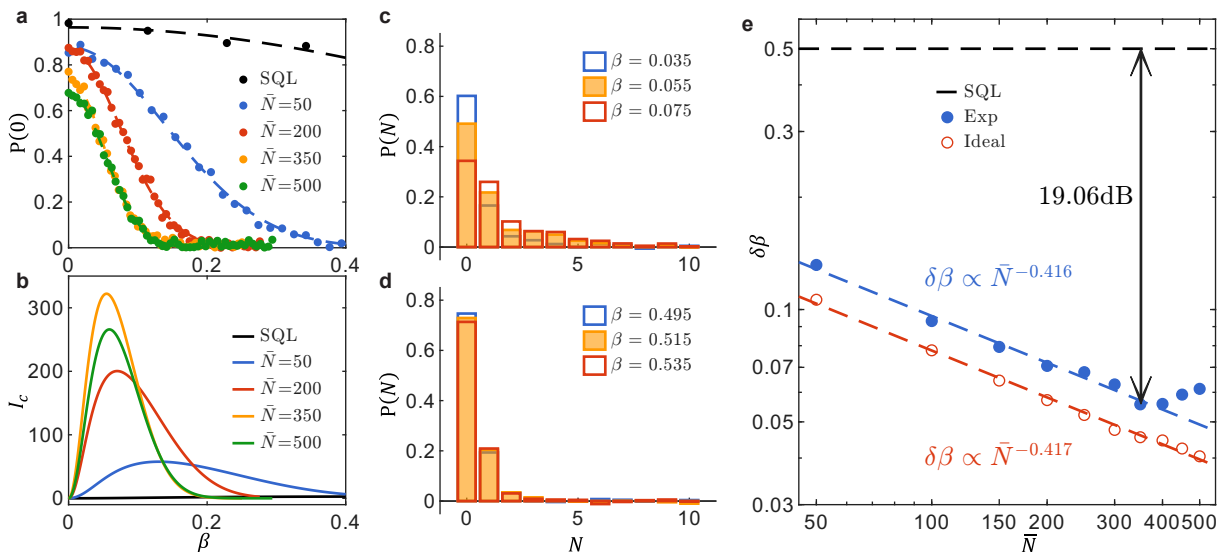


FIG. 4: **Quantum sensing of displacement.** **a**, Measured vacuum population $P(0)$ vs. displacement β . N -focused states (\bar{N} from 50 to 500) show a steeper slope (higher sensitivity) than the coherent state (SQL benchmark). **b**, Fisher Information I_c (derived from **a**) shows a massive quantum enhancement for N -focused states over the coherent state at optimal bias points. **c**, Focused $\bar{N} = 350$ state detection result. The same signal $\delta\beta$ (bottom) induces a dramatic, measurable change in the photon-number distribution of the final state, illustrating the mechanism of quantum gain. **d**, Coherent state (SQL) detection result. A small signal $\delta\beta$ (bottom) causes a negligible change to the final state. **e**, Displacement sensitivity $\delta\beta$ versus \bar{N} . The N -focused states (blue dots) demonstrate a clear quantum advantage, surpassing the SQL (black dashed line). A maximum quantum gain of 19.06 ± 0.13 dB is achieved at $\bar{N} = 350$. Linear fitting (blue dashed line) reveals that the sensitivity scales as $\bar{N}^{-0.416}$, approaching the Heisenberg-limit scaling ($N^{-0.5}$). This scaling is well-described by lossless simulation (yellow circles and dashed line, $\bar{N}^{-0.417}$).

as shown by the black dashed line in Fig. 4(e). The ratio $10 \log_{10} (|\delta\beta_{\text{SQL}}/\delta\beta|)^2$ defines the quantum metrology gain in decibels. The minimum $|\delta\beta|$ measured experimentally occurs at $\bar{N} = 350$, where $|\delta\beta| \geq 0.0557$, corresponding to a 19.06 ± 0.13 dB gain over coherent states. Further increasing the photon number leads to an increase in $|\delta\beta|$, as the benefits of increased \bar{N} are gradually overcome by the increased photon-loss rate within the high-photon-number range.

By fitting the experimental data for $\bar{N} < 350$ and the simulation data, we find that the measurement precision varies with the average photon number as $\delta\beta \propto \bar{N}^{-0.416}$. This result is a clear demonstration of near-Heisenberg-limited (HL) scaling, which for an ideal Fock state probe is $\delta\beta_{\text{HL}} \propto N^{-0.5}$. We also numerically simulate the maximum precision of the confocal circuit under lossless conditions, as shown by the circles in Fig. 4(e). The simulated measurement precision scales with \bar{N} as $\delta\beta \propto \bar{N}^{-0.417}$, which agrees well with the experimental result. The lossless simulation indicates that the measurement precision can be further improved by extending the cavity lifetime. Our results confirm that the quantum confocal microscope in Fock space is highly effective and scalable.

III. DISCUSSION

In this work, we have introduced the concept of quantum confocal microscopy in Fock space and demonstrated it experimentally as a unified framework for the deterministic prepa-

ration, manipulation, and detection of non-classical bosonic states at macroscopic photon numbers. In a superconducting circuit QED platform, merely requiring Kerr nonlinearity and weak driving, we have successfully realized a 4f confocal microscopy and prepared N -focused states with up to 500 photons, demonstrating the scalability of the approach. Utilizing the latter half of the confocal system, we implement Fock-space scanning tomography to detect the photon-number distribution of unknown states, achieving excellent agreement with theory. Finally, we employ the complete confocal circuit for displacement sensing, achieving a quantum-enhanced precision exceeding the SQL by 19 dB. Our experiment provides a scalable method for leveraging high-photon-number states in quantum metrology. Requiring only the elementary nonlinearity of a bosonic resonator and vacuum-state detection, our approach is highly adaptable to a wide range of other bosonic architectures, such as acoustic [33], optomechanical [50], trapped ions [20], and cavity QED systems [46, 51, 52], for quantum-enhanced sensing of diverse physical parameters.

The primary source of dissipation in this experiment is single-photon loss in the high-photon-number range. Due to the bosonic nature of photons, the lifetime of a Fock state $|N\rangle$ scales inversely with photon number, $T_1 \propto 1/N$. However, the phase accumulation time of the confocal lens system is determined by the paraxial condition (Supplementary Section I) and scales as $T_L \propto 1/\sqrt{\bar{N}}$ [45]. Consequently, the total execution time of the confocal circuit decreases with \bar{N} for a fixed

Kerr nonlinearity, partially mitigating the impact of single-photon dissipation. We anticipate that even higher metrological gain is possible by further optimizing the lifetime of the cavity [53]. In experimental systems, the Kerr nonlinearity strength often depends on \bar{N} . Designing specialized nonlinear devices to maintain or even enhance the Kerr nonlinearity in the high-photon-number range [54] offers a promising path toward improving circuit efficiency and metrological performance.

* These authors contributed equally to this work.

† Electronic address: lmwin@ustc.edu.cn

‡ Electronic address: clzou321@ustc.edu.cn

§ Electronic address: luyansun@tsinghua.edu.cn

- [1] R. Schnabel, N. Mavalvala, D. E. McClelland, and P. K. Lam, “Quantum metrology for gravitational wave astronomy,” *Nat. Commun.* **1**, 121 (2010).
- [2] K. M. Backes, D. A. Palken, S. A. Kenany, B. M. Brubaker, S. B. Cahn, A. Droster, G. C. Hilton, S. Ghosh, H. Jackson, S. K. Lamoreaux, *et al.*, “A quantum enhanced search for dark matter axions,” *Nature* **590**, 238 (2021).
- [3] Y. Wang, Y. Huang, X. Kang, D. Chang, J. Xu, Y. Chen, S. Pustelny, W. Zheng, M. Jiang, X. Peng, *et al.*, “Constraints on axion dark matter by distributed intercity quantum sensors,” *Nature* **650**, 314 (2026).
- [4] V. Giovannetti, S. Lloyd, and L. Maccone, “Quantum-enhanced measurements: Beating the standard quantum limit,” *Science* **306**, 1330 (2004).
- [5] V. Giovannetti, S. Lloyd, and L. Maccone, “Advances in quantum metrology,” *Nat. Photonics* **5**, 222 (2011).
- [6] J. Huang, M. Zhuang, and C. Lee, “Entanglement-enhanced quantum metrology: From standard quantum limit to heisenberg limit,” *Appl. Phys. Rev.* **11**, 031302 (2024).
- [7] L. Jiao, W. Wu, S.-Y. Bai, and J.-H. An, “Quantum metrology in the noisy intermediate-scale quantum era,” *Adv. Quantum Technol.* **8**, 2300218 (2025).
- [8] V. Montenegro, C. Mukhopadhyay, R. Yousefjani, S. Sarkar, U. Mishra, M. G. A. Paris, and A. Bayat, “Review: Quantum metrology and sensing with many-body systems,” *Phys. Rep.* **1134**, 1 (2025).
- [9] C. Mukhopadhyay, V. Montenegro, and A. Bayat, “Current trends in global quantum metrology,” *J. Phys. A: Math. Theor.* **58**, 063001 (2025).
- [10] K. C. Cox, G. P. Greve, J. M. Weiner, and J. K. Thompson, “Deterministic squeezed states with collective measurements and feedback,” *Phys. Rev. Lett.* **116**, 093602 (2016).
- [11] O. Hosten, N. J. Engelsens, R. Krishnakumar, and M. A. Kasevich, “Measurement noise 100 times lower than the quantum-projection limit using entangled atoms,” *Nature* **529**, 505 (2016).
- [12] D. Leibfried, M. D. Barrett, T. Schaetz, J. Britton, J. Chiaverini, W. M. Itano, J. D. Jost, C. Langer, and D. J. Wineland, “Toward heisenberg-limited spectroscopy with multiparticle entangled states,” *Science* **304**, 1476 (2004).
- [13] L. Pezzè, A. Smerzi, M. K. Oberthaler, R. Schmied, and P. Treutlein, “Quantum metrology with nonclassical states of atomic ensembles,” *Rev. Mod. Phys.* **90**, 035005 (2018).
- [14] G. P. Greve, C. Luo, B. Wu, and J. K. Thompson, “Entanglement-enhanced matter-wave interferometry in a high-finesse cavity,” *Nature* **610**, 472 (2022).
- [15] T.-W. Mao, Q. Liu, X.-W. Li, J.-H. Cao, F. Chen, W.-X. Xu, M. K. Tey, Y.-X. Huang, and L. You, “Quantum-enhanced sensing by echoing spin-nematic squeezing in atomic bose-einstein condensate,” *Nat. Phys.* **19**, 1585 (2023).
- [16] W. H. Zurek, “Sub-planck structure in phase space and its relevance for quantum decoherence,” *Nature* **412**, 712 (2001).
- [17] S. Pirandola, B. R. Bardhan, T. Gehring, C. Weedbrook, and S. Lloyd, “Advances in photonic quantum sensing,” *Nat. Photonics* **12**, 724 (2018).
- [18] K. C. McCormick, J. Keller, S. C. Burd, D. J. Wineland, A. C. Wilson, and D. Leibfried, “Quantum-enhanced sensing of a single-ion mechanical oscillator,” *Nature* **572**, 86 (2019).
- [19] W. Wang, Y. Wu, Y. Ma, W. Cai, L. Hu, X. Mu, Y. Xu, Z.-J. Chen, H. Wang, Y. P. Song, *et al.*, “Heisenberg-limited single-mode quantum metrology in a superconducting circuit,” *Nat. Commun.* **10**, 4382 (2019).
- [20] F. Wolf, C. Shi, J. C. Heip, M. Gessner, L. Pezzè, A. Smerzi, M. Schulte, K. Hammerer, and P. O. Schmidt, “Motional fock states for quantum-enhanced amplitude and phase measurements with trapped ions,” *Nat. Commun.* **10**, 2929 (2019).
- [21] W. Wang, Z. J. Chen, X. Liu, W. Cai, Y. Ma, X. Mu, X. Pan, Z. Hua, L. Hu, Y. Xu, *et al.*, “Quantum-enhanced radiometry via approximate quantum error correction,” *Nat. Commun.* **13**, 3214 (2022).
- [22] X. Deng, S. Li, Z.-J. Chen, Z. Ni, Y. Cai, J. Mai, L. Zhang, P. Zheng, H. Yu, C.-L. Zou, *et al.*, “Quantum-enhanced metrology with large fock states,” *Nat. Phys.* **20**, 1874 (2024).
- [23] B. Vlastakis, G. Kirchmair, Z. Leghtas, S. E. Nigg, L. Frunzio, S. M. Girvin, M. Mirrahimi, M. H. Devoret, and R. J. Schoelkopf, “Deterministically encoding quantum information using 100-photon schrodinger cat states,” *Science* **342**, 607 (2013).
- [24] X. Pan, T. Krisnanda, A. Duina, K. Park, P. Song, C. Y. Fontaine, A. Copetudo, R. Filip, and Y. Y. Gao, “Realization of versatile and effective quantum metrology using a single bosonic mode,” *PRX Quantum* **6**, 010304 (2025).
- [25] P. Zheng, Y. Cai, B. Xu, S. Wen, L. Zhang, Z. Ni, J. Mai, Y. Zeng, L. Lin, L. Hu, X. Deng, S. Liu, J. Shu, Y. Xu, and D. Yu, “Quantum-enhanced dark matter detection using schrödinger cat states,” *arXiv: 2507.23538* (2025).
- [26] T. Nagata, R. Okamoto, J. L. O’Brien, K. Sasaki, and S. Takeuchi, “Beating the standard quantum limit with four-entangled photons,” *Science* **316**, 726 (2007).
- [27] S. Slussarenko, M. M. Weston, H. M. Chrzanowski, L. K. Shalm, V. B. Verma, S. W. Nam, and G. J. Pryde, “Unconditional violation of the shot-noise limit in photonic quantum metrology,” *Nat. Photonics* **11**, 700 (2017).
- [28] B. M. Escher, R. L. de Matos Filho, and L. Davidovich, “General framework for estimating the ultimate precision limit in noisy quantum-enhanced metrology,” *Nat. Phys.* **7**, 406 (2011).
- [29] R. Demkowicz-Dobrzański, J. Kołodyński, and M. Guţă, “The elusive heisenberg limit in quantum-enhanced metrology,” *Nat. Commun.* **3**, 1063 (2012).
- [30] M. Hofheinz, E. M. Weig, M. Ansmann, R. C. Bialczak, E. Lucero, M. Neeley, A. D. O’Connell, H. Wang, J. M. Martinis, and A. N. Cleland, “Generation of fock states in a superconducting quantum circuit,” *Nature* **454**, 310 (2008).
- [31] H. Wang, M. Hofheinz, M. Ansmann, R. C. Bialczak, E. Lucero, M. Neeley, A. D. O’Connell, D. Sank, J. Wenner, A. N. Cleland, *et al.*, “Measurement of the decay of fock states in a superconducting quantum circuit,” *Phys. Rev. Lett.* **101**, 240401 (2008).
- [32] M. Hofheinz, H. Wang, M. Ansmann, R. C. Bialczak,

- E. Lucero, M. Neeley, A. D. O’Connell, D. Sank, J. Wenner, J. M. Martinis, *et al.*, “Synthesizing arbitrary quantum states in a superconducting resonator,” *Nature* **459**, 546 (2009).
- [33] Y. Chu, P. Kharel, T. Yoon, L. Frunzio, P. T. Rakich, and R. J. Schoelkopf, “Creation and control of multi-phonon fock states in a bulk acoustic-wave resonator,” *Nature* **563**, 666 (2018).
- [34] N. Khaneja, T. Reiss, C. Kehlet, T. Schulte-Herbrüggen, and S. J. Glaser, “Optimal control of coupled spin dynamics: design of nmr pulse sequences by gradient ascent algorithms,” *J. Magn. Reson.* **172**, 296 (2005).
- [35] R. W. Heeres, B. Vlastakis, E. Holland, S. Krastanov, V. V. Albert, L. Frunzio, L. Jiang, and R. J. Schoelkopf, “Cavity state manipulation using photon-number selective phase gates,” *Phys. Rev. Lett.* **115**, 137002 (2015).
- [36] S. Krastanov, V. V. Albert, C. Shen, C.-L. Zou, R. W. Heeres, B. Vlastakis, R. J. Schoelkopf, and L. Jiang, “Universal control of an oscillator with dispersive coupling to a qubit,” *Phys. Rev. A* **92**, 040303 (2015).
- [37] R. W. Heeres, P. Reinhold, N. Ofek, L. Frunzio, L. Jiang, M. H. Devoret, and R. J. Schoelkopf, “Implementing a universal gate set on a logical qubit encoded in an oscillator,” *Nat. Commun.* **8**, 94 (2017).
- [38] A. Eickbusch, V. Sivak, A. Z. Ding, S. S. Elder, S. R. Jha, J. Venkatraman, B. Royer, S. M. Girvin, R. J. Schoelkopf, and M. H. Devoret, “Fast universal control of an oscillator with weak dispersive coupling to a qubit,” *Nat. Phys.* **18**, 1464 (2022).
- [39] W. Wang, L. Hu, Y. Xu, K. Liu, Y. Ma, S.-B. Zheng, R. Vijay, Y. P. Song, L. M. Duan, and L. Sun, “Converting quasiclassical states into arbitrary fock state superpositions in a superconducting circuit,” *Phys. Rev. Lett.* **118**, 223604 (2017).
- [40] E. Davis, G. Bentsen, and M. Schleier-Smith, “Approaching the heisenberg limit without single-particle detection,” *Phys. Rev. Lett.* **116**, 053601 (2016).
- [41] S. Colombo, E. Pedrozo-Peñañiel, A. F. Adiyatullin, Z. Li, E. Mendez, C. Shu, and V. Vuletić, “Time-reversal-based quantum metrology with many-body entangled states,” *Nat. Phys.* **18**, 925 (2022).
- [42] Z. Li, S. Colombo, C. Shu, G. Velez, S. Pilatowsky-Cameo, R. Schmied, S. Choi, M. Lukin, E. Pedrozo-Peñañiel, and V. Vuletić, “Improving metrology with quantum scrambling,” *Science* **380**, 1381 (2023).
- [43] K. A. Gilmore, M. Affolter, R. J. Lewis-Swan, D. Barberena, E. Jordan, A. M. Rey, and J. J. Bollinger, “Quantum-enhanced sensing of displacements and electric fields with two-dimensional trapped-ion crystals,” *Science* **373**, 673 (2021).
- [44] Y. Xu, Y. Zhou, Z. Hua, L. Sun, J. Zhou, W. Wang, W. Cai, H. Huang, L. Xiao, G. Xue, *et al.*, “Principles of optics in the fock space: Scalable manipulation of giant quantum states,” [arXiv:2601.10325](https://arxiv.org/abs/2601.10325) (2026).
- [45] M. Li, W. Cai, Z. Hua, Y. Xu, Y. Zhou, Z.-J. Chen, X.-B. Zou, G.-C. Guo, L. Sun, and C.-L. Zou, “Scalable generation of macroscopic fock states exceeding 10,000 photons,” [arXiv:2601.05118](https://arxiv.org/abs/2601.05118) (2026).
- [46] A. Wallraff, D. I. Schuster, A. Blais, L. Frunzio, R. S. Huang, J. Majer, S. Kumar, S. M. Girvin, and R. J. Schoelkopf, “Strong coupling of a single photon to a superconducting qubit using circuit quantum electrodynamics,” *Nature* **431**, 162 (2004).
- [47] J. Koch, T. M. Yu, J. Gambetta, A. A. Houck, D. I. Schuster, J. Majer, A. Blais, M. H. Devoret, S. M. Girvin, and R. J. Schoelkopf, “Charge-insensitive qubit design derived from the cooper pair box,” *Phys. Rev. A* **76**, 042319 (2007).
- [48] A. Blais, A. L. Grimsmo, S. M. Girvin, and A. Wallraff, “Circuit quantum electrodynamics,” *Rev. Mod. Phys.* **93**, 025005 (2021).
- [49] D. I. Schuster, A. A. Houck, J. A. Schreier, A. Wallraff, J. M. Gambetta, A. Blais, L. Frunzio, J. Majer, B. Johnson, M. H. Devoret, *et al.*, “Resolving photon number states in a superconducting circuit,” *Nature* **445**, 515 (2007).
- [50] S. Barzanjeh, A. Xuereb, S. Gröblacher, M. Paternostro, C. A. Regal, and E. M. Weig, “Optomechanics for quantum technologies,” *Nat. Phys.* **18**, 15 (2022).
- [51] A. Blais, R.-S. Huang, A. Wallraff, S. M. Girvin, and R. J. Schoelkopf, “Cavity quantum electrodynamics for superconducting electrical circuits: An architecture for quantum computation,” *Phys. Rev. A* **69**, 062320 (2004).
- [52] P. Yang, M. Li, X. Han, H. He, G. Li, C.-L. Zou, P. Zhang, Y. Qian, and T. Zhang, “Non-reciprocal cavity polariton with atoms strongly coupled to optical cavity,” *Laser Photonics Rev.* **17**, 2200574 (2023).
- [53] O. Milul, B. Guttel, U. Goldblatt, S. Hazanov, L. M. Joshi, D. Chausovsky, N. Kahn, E. Çiftçürek, F. Lafont, and S. Rosenblum, “Superconducting cavity qubit with tens of milliseconds single-photon coherence time,” *PRX Quantum* **4**, 030336 (2023).
- [54] Z. Hua, Y. Xu, W. Wang, Y. Ma, J. Zhou, W. Cai, H. Ai, Y.-x. Liu, M. Li, C.-L. Zou, *et al.*, “Engineering the nonlinearity of bosonic modes with a multiloop squid,” *Phys. Rev. Appl.* **23**, 054031 (2025).

Acknowledgment

This work was funded by the National Natural Science Foundation of China (Grants No. 12550006, 92265210, 92365301, 92565301, 92165209, 12547179, 12574539, 12474498, 12404567, and 12504580) and the Quantum Science and Technology-National Science and Technology Major Project (2021ZD0300200 and 2024ZD0301500). This work is also supported by the Fundamental Research Funds for the Central Universities, the USTC Research Funds of the Double First-Class Initiative, the supercomputing system in the Supercomputing Center of USTC, and the USTC Center for Micro and Nanoscale Research and Fabrication.

Author contributions

Z.H., M.L., and C.-L.Z. conceived the experiment and provided theoretical support. Z.H., C.M., and Y.Z. performed the experiment, analyzed the data, and carried out the numerical simulations under the supervision of L.S. Y.X., Z.C., and W.C. provided theoretical support. J.C. helped to calibrate the system. Y.X., L.X., H.H., and W.W. contributed to experimental support. Z.H. designed the 3D cavity. H.L. and H.W. fabricated the tantalum transmon qubits. Z.H., C.M., Y.Z., M.L., C.-L.Z., and L.S. wrote the manuscript with input from all authors. C.-L.Z. and L.S. supervised the project.

Competing interests

The authors declare no competing interests.

Correspondence and requests for materials should be addressed to M.L., C.-L.Z., or L.S.